Electronic Supplementary Material (ESI) for Materials Chemistry Frontiers.

Supporting Information

for

Gel-Emulsion Templated Polymeric Aerogels for Solar-Driven Interfacial Water Evaporation Distillation and Electricity Generation

Jianfei Liu,[a] Xiangli Chen,[b] Hui Yang,[a] Jiaqi Tang,[a] Rong Miao,[a] Kaiqiang Liu,[a] and Yu Fang [a]*

a) Key Laboratory of Applied Surface and Colloid Chemistry, Ministry of Education, School of Chemistry and Chemical Engineering, Shaanxi Normal University, Xi'an 710119, P. R. China.

b) Key Laboratory of Chemical Additives for China National Light Industry, Shaanxi Key Laboratory of Chemical Additives for Industry, College of Chemistry & Chemical Engineering, Shaanxi University of Science & Technology, Xi'an, 710021, China.

E-mail: yfang@snnu.edu.cn.

Contents

1. Characterization and Measurement 3

1.1 Characterization of the Gel-emulsion 3

1.2 Rheological Measurements 3

1.3 SEM Observations 3

1.4 FTIR Measurements 3

1.5 Porosity Measurements 4

1.6 Mechanical Property Tests 4

1.7 Characterization of the Carbonized Aerogels 4

2. Supplementary Figures and Tables 6

Movie S1: Showing simultaneous generation of electricity and clean water.

1. Characterization and Measurement

1.1 Characterization of the Gel-emulsion

Confocal laser scanning fluorescence microscopic image of the gel emulsion was taken on a TCS SP5 laser scanning confocal microscope. The structure of the probe used in the observation is shown in **Scheme S1**. The observation was conducted by taking 365 nm as the excitation and 550 nm as the emission wavelengths.

1.2 Rheological Measurements

Rheological measurements were carried out with a stress-controlled rheometer (TA Instruments AR-G2) equipped with steel-coated parallel-plate geometry (20 mm diameter). The gap distance was fixed at 1000 μm. A steel cover matching with a parallel plate was used to avoid evaporation. All measurements were conducted at ambient temperature (25 °C). First, a stress sweep measurement at a fixed frequency (1 Hz) was conducted in a stress range of 0.1-1,000 Pa, which illustrates the mechanical strength of the gel sample.

1.3 SEM Observation

Sizes of the pores and pore throats of the as-prepared porous polymeric monoliths were semi-quantitatively calculated using images taken by a Quanta 200 scanning electron microscope (Philips-FEI, 15 kV and 10 mA). The correction for the average value taken from a random section through a sphere has been applied. Prior to observation, approximately 1 cm^3 of the material was mounted on a sample holder and sputtered with gold for 80 s to ensure sufficient conductivity.

1.4 FTIR Measurements

FTIR measurements were performed on a Bruker VERTEX70 V infrared spectrometer. The testing wavelength was from 400 to 4000 cm^{-1} with 128 scans for each sample. The KBr pellet was obtained by mixing a small amount of the sample and anhydrous KBr powder. The FTIR measurements were carried out at room temperature.

1.5 Porosity Measurements

Mercury injection methods have been effectively applied to characterize the size and size distribution of the pores and to evaluate their structures. **CM2, CM4, CM6, CM8** were chosen as samples to conduct the measurements. AUTOPORE 9500 was employed as the instrument, which is a product of Micromeritics Instrument (Shanghai) Ltd.

1.6 Mechanical Property Tests

Mechanical properties of aerogels were measured by a Xie Qiang mechanical testing machine (CTM 2500 universal testing machine) at room temperature. All aerogel samples for compression test have a cylindrical shape with 12 mm in diameter and 24 mm in height. All samples were set on the lower plate and were compressed by the upper plate at a strain rate of 8.3%/min

1.7 Characterization of the Carbonized Aerogels

The absorption spectrum was measured by a UV-vis Spectrometer from 200 to 1500 nm (Lambda 35, PerkinElmer, USA). An integrating sphere was used to collect the absorption light. XRD pattern was performed on a Bruker D8 Focus diffraction system using a Cu Kα source (λ=0.154178 nm). Raman spectra were collected at room temperature using an in Via Raman spectrometer (Renishaw, inVia) with a back-scattering geometry using a 532 nm laser-line from an Ar-ion laser. IR images were captured using a FLIR A655 infrared thermography camera. The functional groups on surface were obtained from X-ray Photoelectron Spectroscopy (XPS, AXIS ULTRA from Kratos Analytical Ltd), and the binding energies were calibrated by setting C1s peak at 284.6 eV.

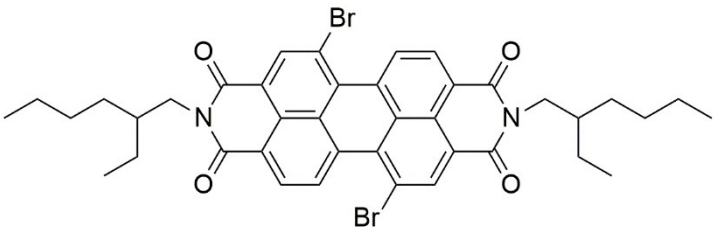

Scheme S1. Structure of the fluorescent probe used for fluorescence imaging.

Table S1. Compositions of the gel-emulsions and the relevant porous polymeric monoliths (**M1-M8**).

No.	Span 80 (*w*/*v*, %)	IA (μL)	DVB (μL)	AIBN (mg)	Dispersed Phase (μL)	Volume Fraction of Dispersed Phase % (*v*/*v*)	Apparent Density (g/cm^3)
M1	1	128	28	20	200	56.2%	0.45
M2	1	128	28	20	300	65.8%	0.39
M3	1	128	28	20	444	74.0%	0.25
M4	1	128	28	20	1000	86.5%	0.2
M5	1	128	28	20	2000	92.7%	0.09
M6	1	128	28	20	3000	95.1%	0.06
M7	1	128	28	20	4000	96.2%	0.04
M8	1	128	28	20	5000	97.0%	0.038

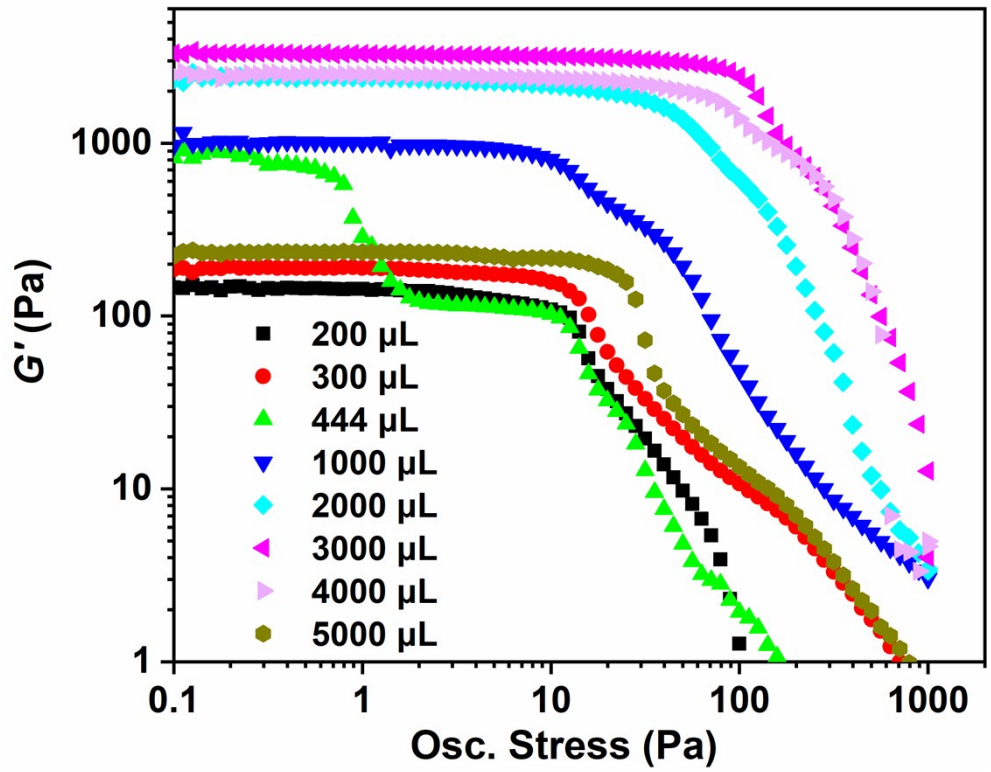

Figure S1. Rheological behaviors of the gel emulsions prepared with different amount of water. Composition of the gel-emulsions was shown in **Table S1**.

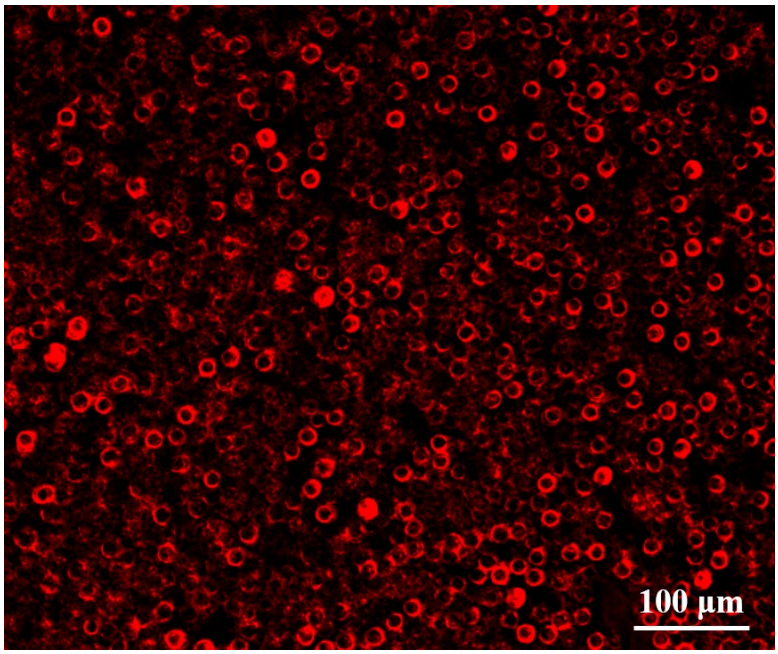

Figure S2. Fluorescence confocal image of the gel emulsion with a water content of 5000 µL, which is the gel emulsion used for preparing **M8** (**Table S1**).

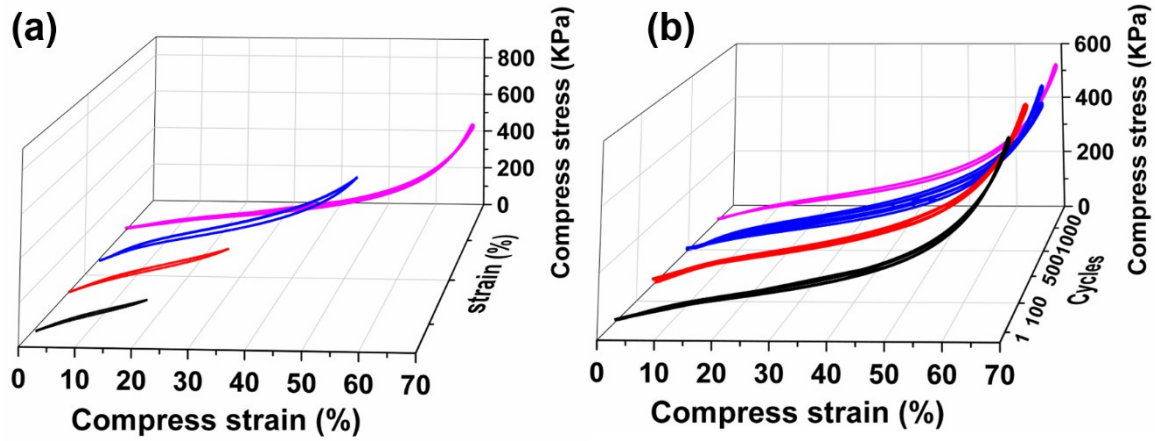

Figure S3. Compressive stress-strain curves of the porous polymeric monoliths with different compress strains (a), where curves in (b) show the compressive performances of **M8** with cycle numbers up to 1000. Detailed compositions are provided in the main text (**Table S1**).

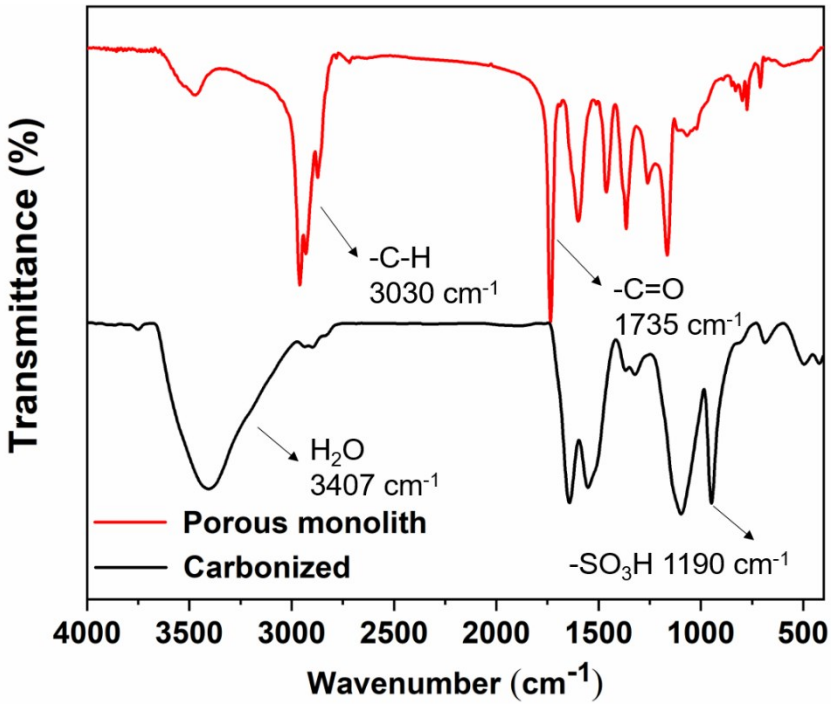

Figure S4. FTIR spectra of a sample pristine aerogel (**M8**) and the corresponding carbonized aerogel (**CM8**).

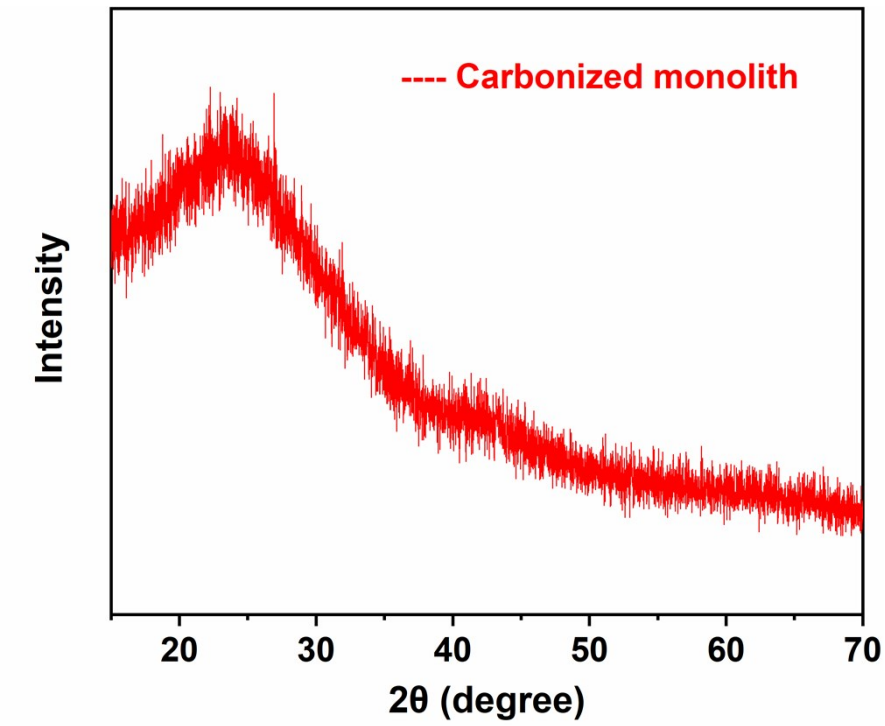

Figure S5. The X-ray diffraction (XRD) pattern of the polymeric monolith from **CM8**, which shows broad peak of amorphous carbon.

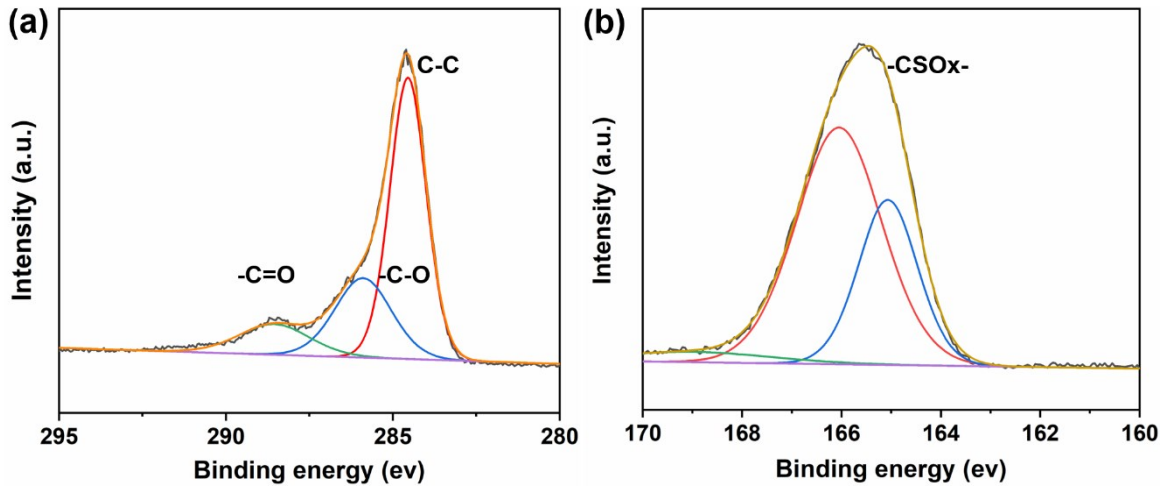

Figure S6. High-resolution XPS spectra of the porous polymeric monolith from **CM8**. (a) C1s and (b) S2p spectra.

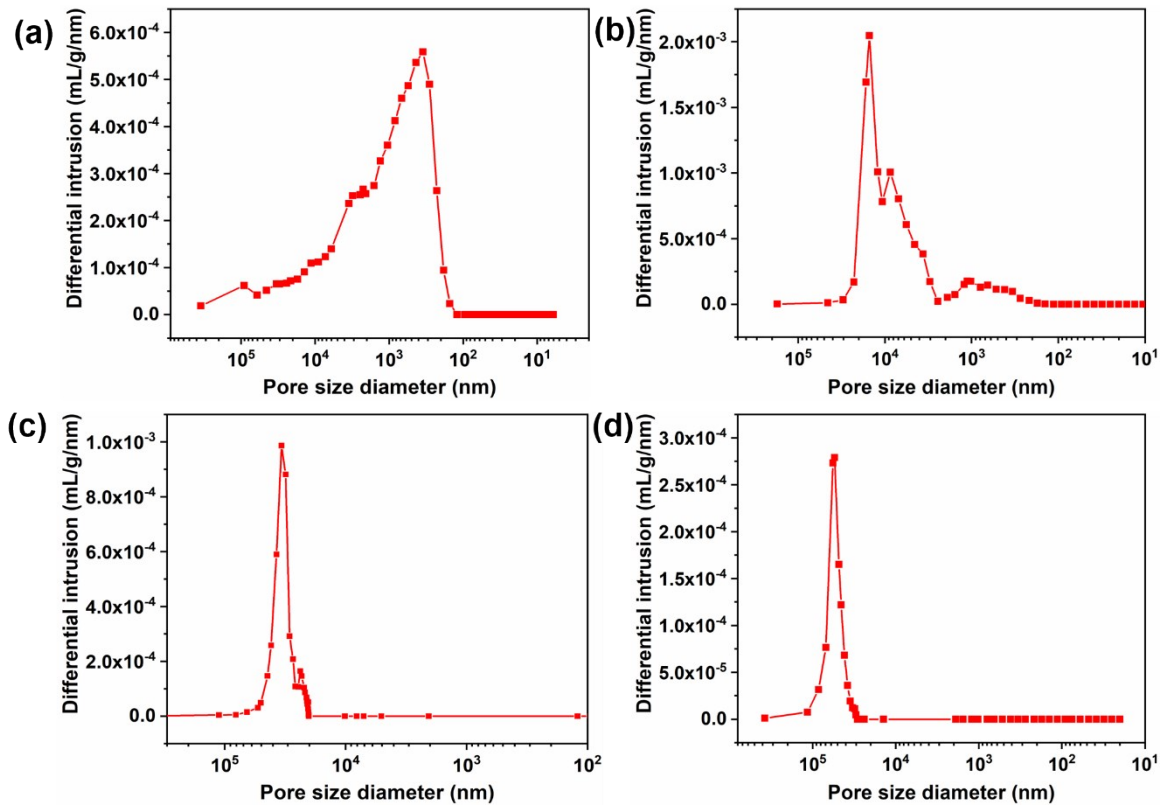

Figure S7. Pore diameter distribution of porous polymeric monoliths from **CM2** (a), **CM4** (b), **CM6** (c), and **CM8** (d), respectively.

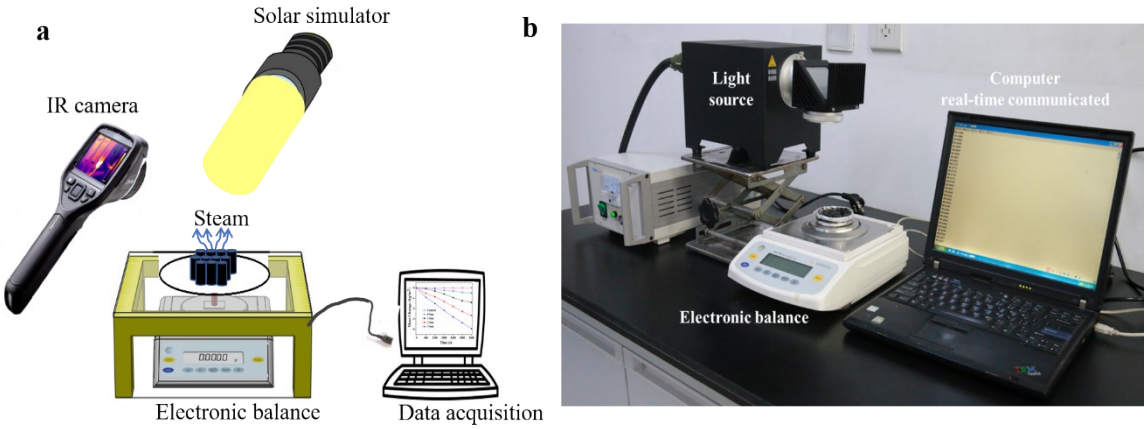

Figure S8. Schematic illustration of the experimental setup for solar vapor generation (a). The experimental set-up of the system (b). The evaporation rate is measured by an electronic balance, which communicates to a laptop computer to record data for monitoring evaporation rate and solar-thermal conversion efficiency.

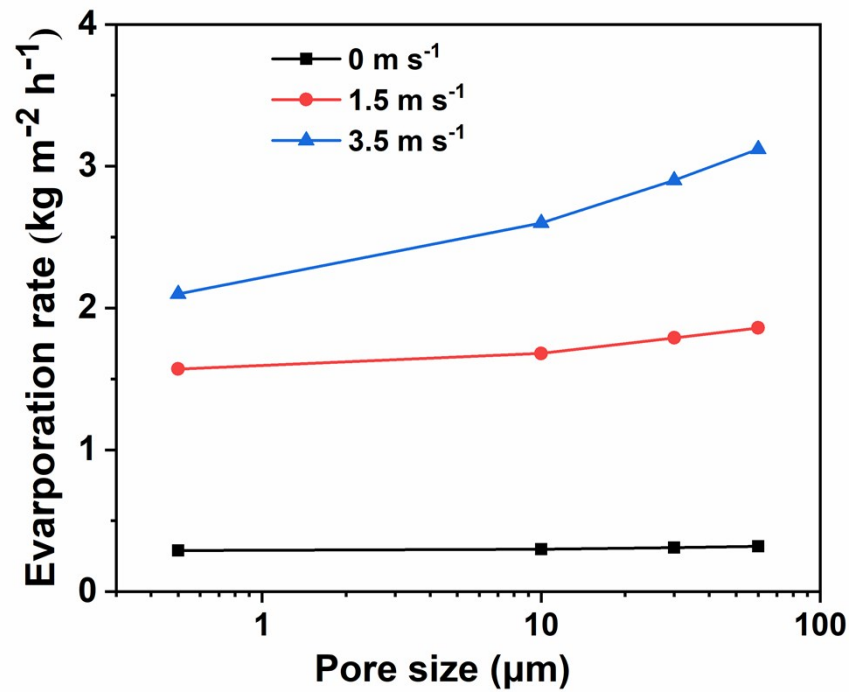

Figure S9. The dependence of evaporation rates of the **CM2**, **CM4**, **CM6** and **CM8** on pore sizes with various convection flows (without sunlight illumination). Evaporators with large pores enable more effective vapor diffusion, thus realizing higher evaporation rates.

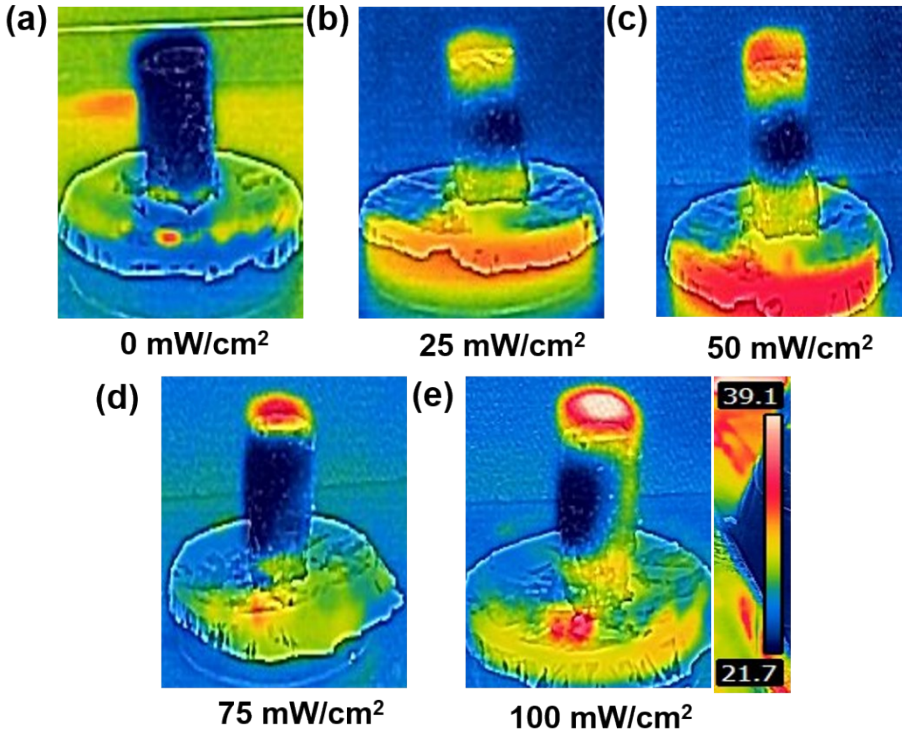

Figure S10. IR thermography images of the carbonized 3D monolith (**CM8**) under different intensities of sunlight illumination. (a) 0 mW/cm^2, (b) 25 mW/cm^2, (c) 50 mW/cm^2, (d) 75 mW/cm^2, and (e) 100 mW/cm^2.

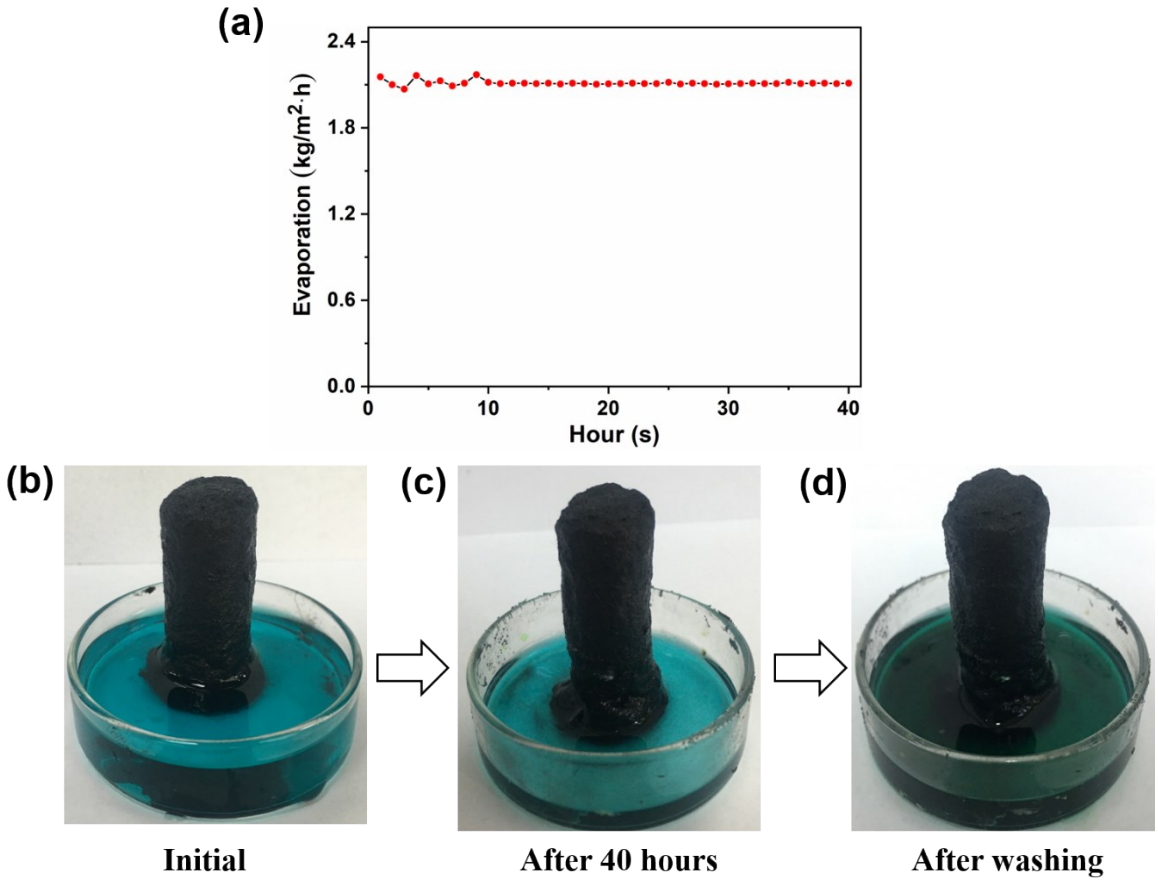

Figure S11. Evaporative durability of the interconnected carbon foam while treating wastewater contaminated by heavy metal ions. (a) The interconnected carbon foam shows a stable evaporation rate during tests. (b-d) Photographs of the interconnected carbonized aerogel while treating wastewater polluted by heavy metal ions.

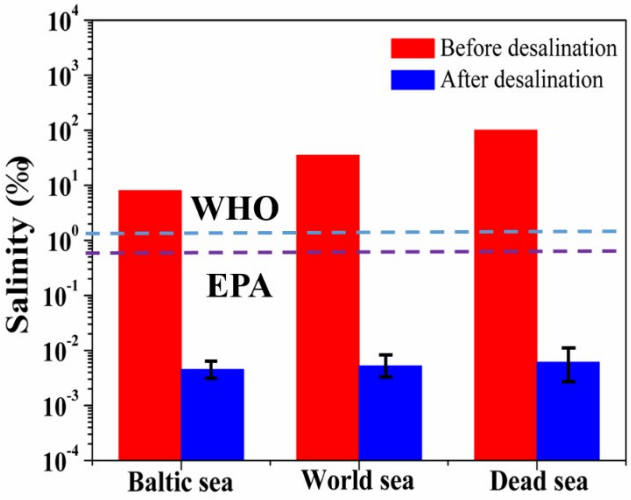

Figure S12. Salinity of the three artificial seawater samples before (red) and after (blue) desalination. The dashed lines are the salinity values approved for drinking water suggested by the World Health Organization (WHO, blue) and US Environmental Protection Agency (EPA, purple).

Note: Three brine samples with different salinities (grams of dissolved salt per kg of seawater) were chosen as the representatives, which are: (1) Baltic Sea (lowest salinity, 8‰), (2) world sea (average salinity, 35‰), and (3) Dead Sea (highest salinity, 100‰).

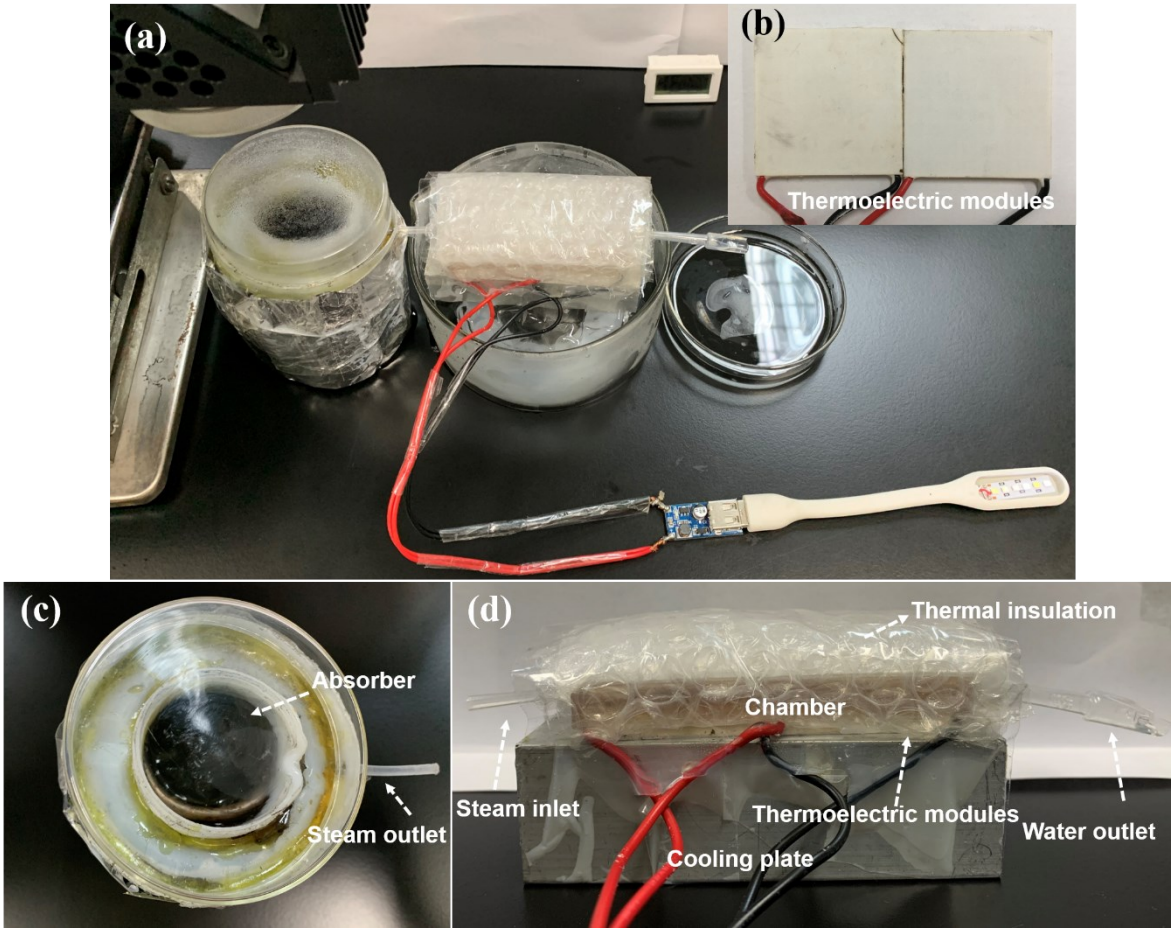

Figure S13. The integrated solar-driven system and the relevant evaporation and electricity generation components. (a) Photos of the real setup of the system. (b) a commercial Bi_2Te_3 thermoelectric module. (c) An optical image of the steam generation device. (d) An optical image of the electricity and water generation part. *Note*: A copper chamber (Length: 8 cm, Width: 4.2 cm, Height: 1 cm) was selected for steam heat exchange.

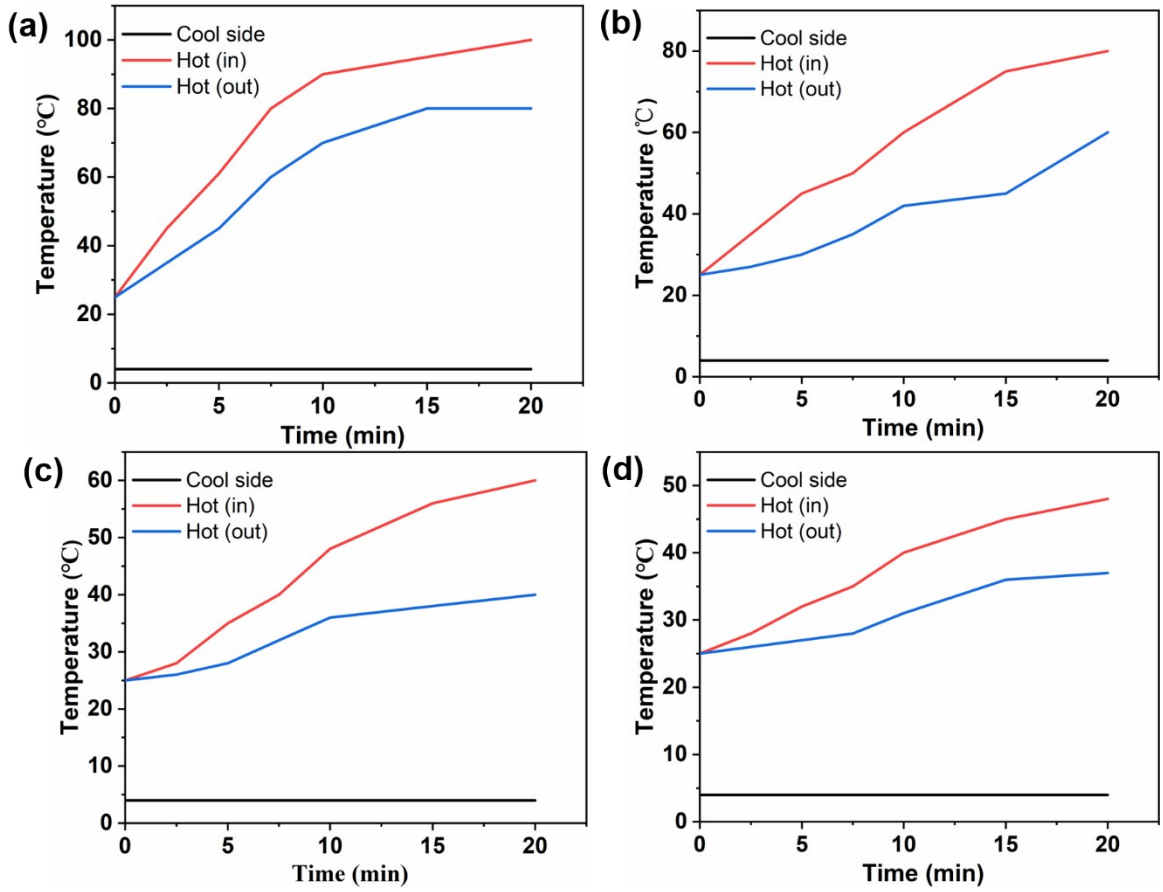

Figure S14. The temperature distribution in thermoelectric device. (a), (b), (c) and (d) represent the temperature distributions and changes under 4, 5, 6 and 9 kW/m^2 sunlight illuminations, respectively, where Hot (in) indicates the temperature of the hot side of the chamber near steam, and Hot (out) represents the temperature of the other end of the chamber. Cool side represents the cooling fin of thermoelectric device.